Journal of Engineering Science and Technology
Vol. 20, No. 3 (2025) 686 - 703

LIZARD-INSPIRED STANDING WAVE QUADRUPEDAL LOCOMOTION FOR SOFT IN-PIPE NAVIGATION ROBOT

GLADY AMEN[1], MOHD SHAHRIMIE MOHD ASAARI[1], MOHAMAD TARMIZI ABU SEMAN[1], MOHAMAD KHAIRI ISHAK[2], ABDUL SATTAR DIN[1,*]

[1]School of Electrical & Electronic Engineering, Universiti Sains Malaysia, Engineering Campus, Seberang Perai Selatan, Nibong Tebal, Penang 14300 Malaysia
[2]Department of Electrical and Computer Engineering, College of Engineering and Information Technology, Ajman University, Ajman, United Arab Emirates
*Corresponding Author: sattar@usm.my

Abstract

Numerous studies have been conducted for in-pipe navigation robots with the sole purpose of navigating through and inspecting pipelines. Most in-pipe navigation robots are of the rigid type. There is an increasing trend to incorporate soft-robotic technology into in-pipe navigation robots. However, most of the soft in-pipe navigation robots' design and locomotion are inspired by inchworm and earthworm, leaving other potential methods of locomotion largely untapped. This paper describes the design and development of a lizard-inspired soft robot to investigate the feasibility of using the lizard-inspired standing wave quadrupedal Locomotion and head stabilization to steadily navigate inside a pipeline. This soft robot is designed and simulated in Solidworks 3D modelling software and fabricated using SORTA-Clear 40 soft silicone rubber using a moulding technique. The soft robot is actuated using pressurized air. A series of experiments are conducted to evaluate the performance of the robot's navigation inside straight pipes of different diameters as well as through pipe corners of different angles. Based on the experiment, the robot achieves a speed of 2.02, 2.77, and 2.33 mms^{-1} inside straight pipes of 50 mm, 60 mm, and 70 mm in diameter, respectively. For navigation through 45° and 90° pipe corners, a navigation speed of 2.94 and 0.73 mms^{-1} has been achieved, respectively. The robot has also demonstrated good head stability with an average side-to-side movement of 3.6 mm from the centre of the pipe and an average head rotation of 6.1° during the locomotion. The results demonstrated the potential of using lizard-inspired locomotion for in-pipe navigation, which has been reported in the literature before.

Keywords: Bioinspired robot, In-pipe navigation robot, Pipe inspection, Silicone rubber, Soft robot.

1. Introduction

Facilities such as petrochemical plants, power plants, and water treatment plants, use pipelines to transport fluids between two destinations. Regular inspection and maintenance are required to ensure that pipelines are in good and safe condition.

Numerous robotic solutions have been developed to navigate inside pipelines to perform inspections. However, most solutions were based on rigid frameworks that were limited in their ability to interact and operate within a dynamic environment [1-6]. Recently, there has been an increasing trend in adopting soft-robotic technology in developing in-pipe navigation robots. Soft robotics is a new branch of robotics where a robot is made entirely of soft and stretchable materials [7, 8]. This type of robot is advantageous compared to the traditional rigid robot in the sense that it is cheaper and more flexible, which enables it to easily adapt to complex and dynamic environments such as those found inside pipelines.

In literature, there have been several in-pipe navigation robots developed based on soft robotic technology, most of which were inspired by either inchworm or earthworm locomotion. An inchworm consists of a fixed front and rear anchor (legs) connected by a bendable middle segment.

The inchworm locomotion sequence starts with releasing the rear legs, bending the middle segment to pull the rear legs forward, securing the rear legs, releasing the front legs, straightening (extending) the middle segment to push the front legs forward, and securing the front legs. Adams et al. [9] developed a waterpipe robot utilising soft inflatable actuators inspired by an inchworm. The robot consists of a retractable telescopic tube with two inflatable anchoring actuators mounted at both ends of the tube. The robot moves by alternatingly inflating the anchoring actuators while controlling the retraction of the middle tube.

Zhang et al. [10] adopted a similar locomotion strategy for their robot. The robot consists of a soft inflatable head and tail, which serve as the front and rear anchor connected by an extensible middle segment. During the locomotion, the tail is anchored while the middle segment is extended longitudinally to push the head forward. Next, the head is anchored, and the tail is released while the middle segment is contracted, pulling the tail forward.

Several inchworm-inspired in-pipe robots adopted a slightly different motion sequence whereby the back anchoring is done concurrently with the middle segment extension whereas the front anchoring is done concurrently with the middle segment contraction. This motion sequence is utilized by Yamamoto et al. [11], Mark et al. [12] and Zhang et al. [13] in their robots. Some other soft in-pipe robots inspired by inchworm locomotion were also found in [14-22].

Aside from the soft in-pipe robots inspired by inchworm locomotion, several other in-pipe robots are inspired by earthworm locomotion. An earthworm's anchors move throughout its body, in contrast to the inchworm's fixed front and back anchors. An earthworm creates an anchor by radially extending certain body portions, which moves from the front to the back of the body like a peristaltic wave [23]. This strategy was adopted by Yamamoto et al. [24] in their in-pipe robot. The robot consists of a long flexible tube with two sliding anchors.

The locomotion starts by holding the back anchor stationary while sliding the front anchor forward along the tube. Next, the front anchor holds the robot

stationary while the back anchor slides forward. Finally, both anchors are held in place while the flexible tube slides forward. Seok et al. [25] developed an earthworm-inspired in-pipe robot consisting of a long soft tube divided into multiple sections. By sequentially contracting multiple sections, the robot generates a travelling wave similar to that of an earthworm. Other earthworm-inspired in-pipe robots can be found in [26-28].

Another researcher developed a soft in-pipe navigation robot inspired by the euglenoid [29]. An euglenoid has an almost similar locomotion strategy as that of the earthworm except that it only has only one anchor that travels along its body. This robot consists of three air chambers connected in series that are inflated sequentially to produce a travelling wave. Niu et al. [30] on the other hand developed a soft in-pipe navigation robot inspired by a caterpillar. A caterpillar moves by generating a transverse wave that moves from the back to the front.

While the majority of the soft in-pipe robots are inspired by biological creatures, few robots employ a completely different locomotion strategy. Takayama et al. [31] developed a twisted bundled tube locomotive device driven by a pneumatic system. As the name suggests, the robot consists of multiple long tubes twisted together to form a bundle. Inflating any of the tubes causes the device to deform into a helix. If these tubes are sequentially pressurized, the device exhibits helical rotation about its body axis while retaining its helical shape. Hu and Li [32] developed an in-pipe robot in the form of an origami flexiball. The robot moves by the alternate flattening and expansion of the flexiball structure.

Current soft in-pipe navigation robots' designs have their advantages and disadvantages. Inchworm-inspired soft in-pipe robots have the advantage of being simple in design and able to produce strong locomotion. This type of robot also has some postural stability on some parts of the robot to allow for inspection instruments to be mounted. The main disadvantage is that the locomotion is non-continuous in the sense that during half of the locomotion cycle, the head of the robot stops when the back anchor is being pulled forward.

The earthworm-inspired and euglenoid-inspired robots can provide postural stability and strong locomotion but are more complicated in terms of the structure and control to produce a smooth travelling anchor along their body. Besides, they also produce non-continuous locomotion. The rest of the robots' design lacks postural stability and produces weak and non-continuous locomotion in addition to being more complicated. All the drawbacks of the current soft in-pipe navigation robots warrant a continuous exploration of new robot designs and locomotion strategies by the research community.

Even though many soft in-pipe navigation robots found in the literature were inspired by inchworm, earthworm, euglenoid, and caterpillar, many other biologically inspired locomotion strategies can be adopted into an in-pipe navigation robot but have not yet been explored. For example, lizard locomotion can be a good alternative to the existing in-pipe locomotion strategy owing to the simple body movement that can be replicated using the soft robotic actuation method.

Furthermore, the quadrupedal locomotion of a lizard coupled with head stabilization has the potential to provide a more continuous movement and postural stability. Some researchers have tried to develop lizard-inspired soft robots, but these robots were designed to walk on flat surfaces. An example of such a robot

can be found in [33, 34]. The robots focus on climbing through adhesion, in which the leg of the robot is attached to a specially designed rubber suction cup to emulate the ability of a gecko to stick to the wall.

The work described in this paper seeks to contribute to the research in soft in-pipe navigation robots by investigating the feasibility of lizard-inspired locomotion for navigation inside pipes, which has not been reported in the literature before. The robot is designed to produce standing wave quadrupedal locomotion coupled with head stabilization to give postural stability to the front part of the robot, which provides stable ground for inspection instruments' mounting. The rest of the paper is organised as follows.

In Section 2, the methodology of the research is presented, which includes the design and Finite Element Analysis (FEA) simulation of the robot, the fabrication, the design of the pneumatic control circuit and algorithm, and the experimental setups to evaluate the performance of the robot inside pipes. The experimental result will be presented and discussed in Section 3 before it is concluded in the following section.

2. Methods

2.1. Robot design

A lizard moves by laterally bending its trunk and lifting its legs in an alternating manner during quadrupedal locomotion. The lateral bending of the trunk creates either a standing wave or a travelling wave depending on the species of lizard [35, 36]. During the bending of the lizard's trunk, one of the hind legs and the opposite front leg are anchored to the ground while the other two legs are lifted and pushed forward. The two lifted legs are then lowered to the ground, followed by the bending of the trunk in the opposite direction. The two previously anchored legs are then lifted and pushed forward. This entire cycle is continuously repeated during locomotion.

In this work, a lizard-inspired soft robot was designed based on the standing wave quadrupedal locomotion because it can be realized with only two air pumps as opposed to the travelling wave locomotion method, which requires more air pumps. The design of the robot is shown in Fig. 1.

The robot was designed using Solidworks 3D modelling software and fabricated using SORTAClear 40 silicone rubber (Smooth-on USA). As shown in Fig. 1(a), the robot consists of four segments, which are the tail, trunk, neck, and head segments. The trunk segment is responsible for the robot's locomotion, whereas the neck segment is responsible for stabilising the lizard's head during locomotion. This feature is desirable for an in-pipe navigation robot as it provides a stable platform on the robot for mounting sensors or cameras for pipe inspection.

The trunk of the robot consists of two inflatable air chambers located on each side of the trunk, separated by a rubber wall in the middle. The two chambers are connected to two separate air pumps using silicone rubber tubes. Inflating only one of the chambers causes the trunk to bend, which mimics the bending of the lizard's trunk. The neck segment is divided into the lower neck and upper neck. Both the lower and upper neck have similar actuation mechanisms in that they have two inflatable air chambers located on each side of the neck. The only difference is in

the length of the segment where the length of the lower neck is about half the length of the trunk segment and the length of the upper neck is half of that of the lower neck. This is to reduce the effect of the trunk bending on the head of the lizard, thus stabilizing it during locomotion.

Each of the air chambers in the lower neck is connected to the opposite air chambers in the trunk, as shown in Fig. 1(b). Similarly, each of the air chambers in the upper neck is connected to the opposite air chamber in the lower neck. Therefore, when one of the chambers on the trunk is inflated, the opposite chamber in the lower neck is also inflated, causing it to bend in the opposite direction of the trunk's bending. At the same time, the chamber in the upper neck that is opposite to the inflated chamber in the lower neck is also inflated, causing it to bend in the opposite direction of the lower neck's bending, as shown in Fig. 1(c).

A pair of hind legs and a pair of front legs are attached to the respective back end and front end of the trunk segment. The leg is designed to be a passive robot structure in that it does not have any actuation mechanism. The leg has a curved design pointing backwards. The outer surface of the leg is covered with an array of rubber spikes pointing forward, as shown in Fig. 1(d). It is designed in such a way that the friction between the leg and the pipe wall is smaller when the leg is being pulled forward and larger when the leg is being pushed backwards. A tail structure is attached to the back end of the trunk to prevent excessive bending of the trunk, which can cause the hind legs to be flipped forward, which can stop the forward motion of the robot.

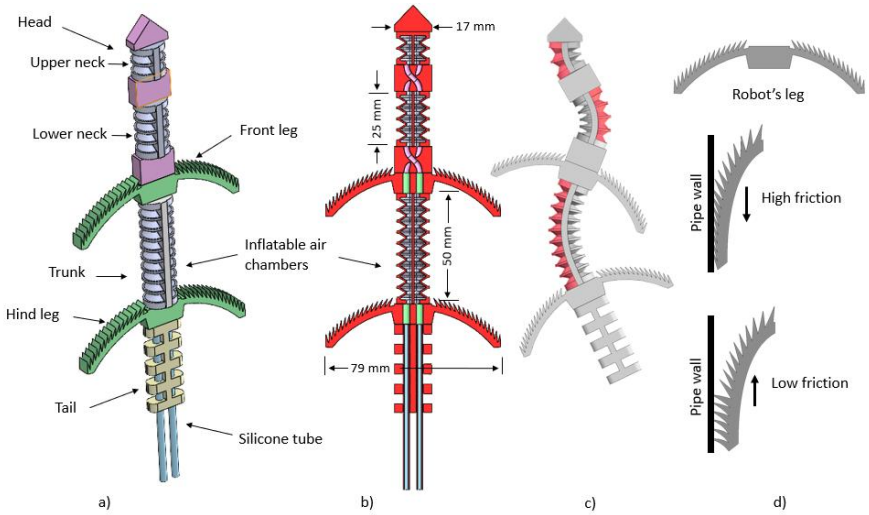

Fig. 1. (a) Robot 3D model, (b) cross-sectional view, (c) effect of chamber inflation (the red chambers are the chambers that are being inflated) and (d) leg design.

The size and dimensions of the robot are chosen based on the size of the available pipe diameters (50 mm, 60 mm, and 70 mm) in which the test will be carried out. Parameters including the length, and the thickness of the chamber wall are optimized using the Finite Element Analysis (FEA) in the Solidworks

modelling software to produce the standing wave that can fit inside the pipe diameters. The sequence of the robot's motion is illustrated in Fig. 2.

Before the start of actuation, the robot's body is in a straight posture. When the actuation starts, one side of the air chamber is inflated, causing the trunk to bend to one side. This causes the hind leg on the same side of the bend (i.e., opposite of the inflated air chamber) and the opposite front leg to be pulled forward. At the same time, the other two legs are pushed backwards. Since the forward pull of the leg has less friction as compared to the backward push, there will be a net forward pull of the legs. The cycle is repeated when the opposite chamber is inflated, causing the trunk to bend to the other side. There is always a net forward pull of the robot's legs in each cycle, which causes the robot to move forward.

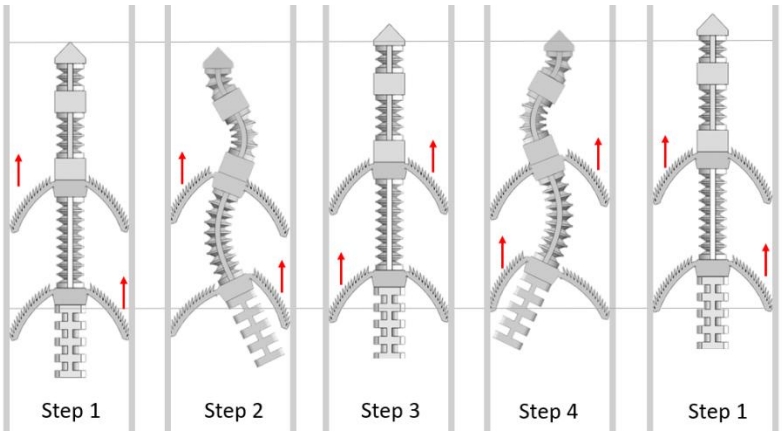

Fig. 2. Robot sequence of motion illustration.

To verify the feasibility of the robot design before it is fabricated, a Finite Element Analysis (FEA) was performed using the Solidworks simulation. A tensile test was performed on the SORTA-Clear 40 silicone rubber samples using an Instron3366 universal tester machine. From the test, a stress-strain curve was obtained as shown in Fig. 3. The average elongation at break is around 310% and the average 100% modulus is recorded at 0.68 MPa. This data was then used to define a new material inside the Solidworks simulation, which was then applied to the robot's 3D model.

The choice of the silicone rubber used to fabricate this robot is based on the shore hardness and the elongation at break, which subsequently determine the air pressure required to actuate the robot. The softer the material, the lower the air pressure required to actuate the robot and vice versa. However, a lower air pressure produces a weaker actuation for the robot whereas the higher air pressure requires a larger and hence, more expensive air pump. A material with higher elongation at break can tolerate a higher deformation without sustaining physical damage and vice versa.

For this project, the 40 on the A scale Shore hardness coupled with the 400% elongation at break provided by the SORTA-Clear 40 silicone rubber is one of the suitable candidates to be used with the existing air pump that can produce air pressure of up to 80 kPa.

A non-linear static FEA simulation was performed on the Solidworks 3D model, and the applied fixtures and loads are shown in Fig. 4(a). A pressure of 50 kPa was applied on the inside walls of the air chambers as depicted by the red arrows in Fig. 4(a). The meshed and the deformed models are shown in Figs. 4(b) and (c) respectively. From the result, the robot's trunk, lower neck, and upper neck produced the desired opposite bending in response to the pressure load applied on the inner wall of the chambers.

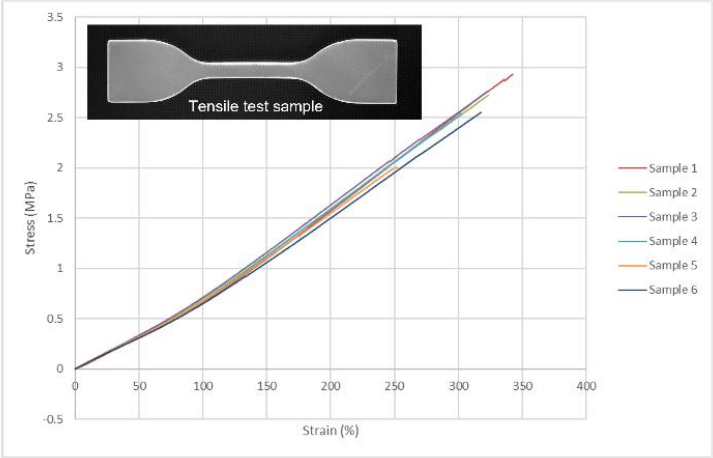

Fig. 3. Stress-strain curve for SORTA-Clear 40. The inset image shows the specimen for the tensile test.

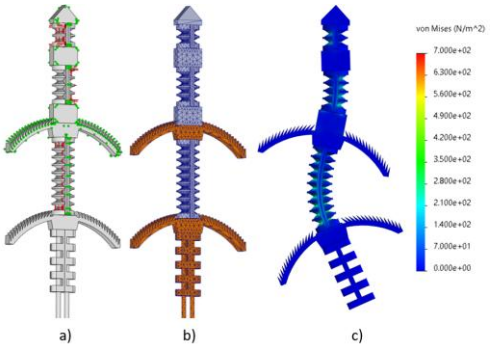

Fig. 4. FEA simulation: (a) Applied load (red arrow) and fixture (green arrow), (b) model mesh, and (c) deformed model with stress value.

2.2. Fabrication

The entire robot's body was fabricated from SORTA-Clear 40 silicone rubber in separate parts, which were then glued together using the same silicone rubber material. These parts are shown in Fig. 5(a). Moulds for each part of the robot were designed using Solidworks and 3D printed using Polylactic acid (PLA) plastic. The SORTA-Clear 40 silicone rubber comes in two parts (A and B), which must be mixed at a ratio of 10:1 by weight. A digital gram scale was used to accurately mix the two parts. The mixture was stirred well for 3 minutes, poured into the PLA moulds, and

left to cure for about 16 hours. Next, the fully cured parts were removed from the moulds and glued together using the same uncured rubber material. The moulding process and the fabricated robot are shown in Figs. 5(b) and (c).

The lizard-inspired soft in-pipe navigation robot was designed to be operated using a pneumatic system as shown in Fig. 6(a). The air chambers on each side of the robot are connected to two separate air pumps via silicone tubing. The air pumps used for the pneumatic system can produce a maximum air pressure of 80 kPa. The silicone tube connecting the air chamber and the pump is also connected to a solenoid valve to release the air. The air pumps and the solenoid valves are controlled using an Arduino nano controller board using the control algorithm shown in Fig. 6(b). A series of experiments were conducted to evaluate the performance of the lizard-inspired soft in-pipe navigation robot.

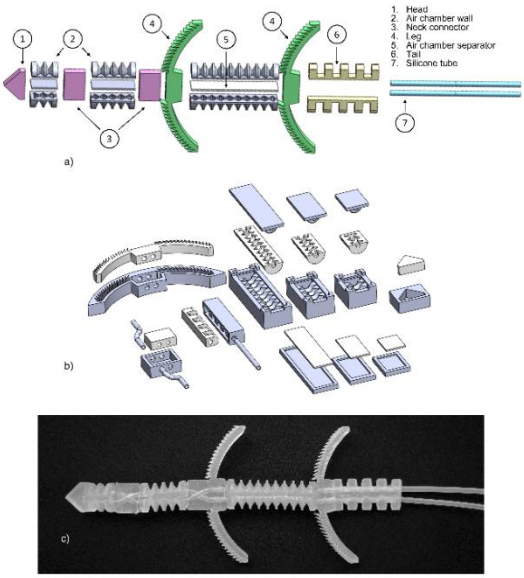

Fig. 5. (a) Robot's 3D parts, (b) moulding process for robot's parts (the grey parts are the mold and the white parts are molded robot parts) and (c) fabricated robot.

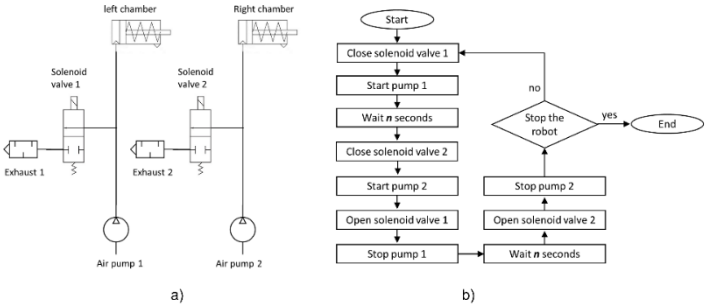

Fig. 6. (a) Pneumatic control diagram and (b) flow chart for the control of the pneumatic system.

2.3. Experimental setup

2.3.1. Experiment 1: Robot's trunk bending radius vs applied pressure

The first experiment was conducted to investigate the effect of air pressure on the bending radius of the robot's trunk. One of the trunk chambers was connected to an air pump through a silicone tube. Pressurized air of different pressure ranges from 0 kPa to 80 kPa was supplied to the trunk's air chamber. For each of the different pressures supplied, the image of the body was captured, and the air pressure was measured using a GM522 pressure manometer (BENETECH). All the images of the bent body were then imported into Solidworks where a curve tool was used to draw a curve on top of the images to follow the exact curvature of the body, as shown in Fig. 7(a). The angle θ of the curve was then recorded. Then, the length of the trunk (curve), l, was used to calculate the radius, r, of the curvature using the following formula:

$$r = \frac{l}{2\pi(360/\theta)} \tag{1}$$

2.3.2. Experiment 2: Leg friction

The second experiment was conducted to test the frictional force between the robot's leg and the pipe wall. Two sets of experiments were conducted: the frictional force during the forward pulling of the leg and the frictional force during the backward pushing of the leg.

The robot's leg was mounted on a stick and inserted into a pipe of 50 mm in diameter as shown in Fig. 7(b). The other end of the stick was mounted on a high-precision digital scale. The pipe was then pushed downward. Due to the frictional force between the leg and the pipe wall, the stick was also pushed downward and pressed against the digital gram scale. The reading of the scale was then recorded. The experiment was repeated with the leg mounted upside-down on the stick to measure the backward frictional force.

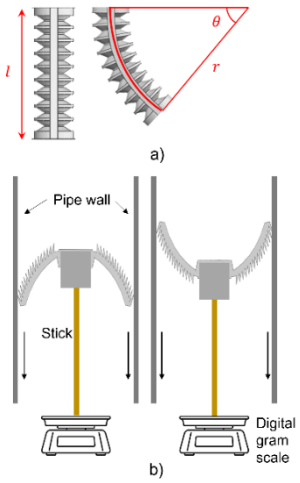

Fig. 7. (a) Bending radius measurement and (b) frictional force experimental setup.

2.3.3. Experiment 3: Navigation performance inside pipe

The third experiment was conducted to evaluate the navigation performance of the lizard-inspired in-pipe robot in straight pipes of different diameters and through pipe corners. The three performance characteristics evaluated were speed, and head stability in terms of lateral movement and lateral rotation. For this experiment, the robot was placed inside a horizontal transparent acrylic pipe of 50 mm in diameter and 50 cm in length. Two spherical markers were placed on the shoulder and the head of the robot. A camera was placed above the pipe to record a video of the robot moving inside the pipe. The robot was actuated according to the control algorithm described in Fig. 6(b), where the n inside the algorithm was set to 1 s and the pump pressure was set to 80 kPa. The robot was left to move from one end of the pipe to the other end. The video was then processed using the MATLAB image processing toolbox to obtain the speed of the robot. The formula for the robot's speed is as follows:

$$v_{vertical} = \frac{FR\_V_n - FR\_V_{n-1}}{N\_V_{pipe\_length}} \times L_{pipe} \times FR\_rate \quad (2)$$

where the FR_V_n and the FR_V_{n-1} are the vertical pixel coordinates of the marker in the current and previous frames, $N\_V_{pipe\_length}$ is the number of vertical pixels for the entire pipe length, L_{pipe} is the actual length of the pipe in mm, and the FR_rate is the video framerate.

The same experiment was conducted for straight pipes of 60 mm and 70 mm in diameter, as well as inside corners of 45° and 90° angles using the same air pressure and timing setting. For the experiment inside corners, the pipe with 60 mm was used. All the pipes used in the experiment are 50 cm in length. The same video was also used to compute the lateral movement of the head and shoulder of the robot to evaluate the stability of the robot head during the robot's locomotion inside a pipeline. The same MATLAB functions were used to track the coordinates of the markers on the head and the shoulder. But for the lateral distance, the actual width (outer diameter) of the pipe was used as a reference to convert the distance in pixels to millimetres.

The lateral distance was calculated from the centre of the pipe by using the following formula:

$$d_{lateral} = \frac{H\_Co_{marker} - H\_Co_{pipe\_center}}{N\_V_{pipe\_diameter}} \times D_{pipe} \quad (3)$$

where H_Co_{marker} and $H\_Co_{pipe\_center}$ are the horizontal pixel coordinates of the marker and the horizontal pixel coordinates of the centre of the pipe respectively, $N\_V_{pipe\_diameter}$ is the number of pixels in one diameter of the pipe, and D_{pipe} is the actual diameter of the pipe in mm. The lateral rotation of the robot was also calculated from the same video using MATLAB. For the rotation of the head and shoulder of the robot, the orientation of the edge of the robot's head and shoulder. The angle was calculated with respect to the longitudinal axis of the pipe.

3. Results and Discussion

Figure 8 shows the result of the trunk's bending experiment. The bending radius was calculated using Eq. (1). Based on the plotted data, at the initial 10 kPa, the bending radius is about 201 mm. As the pressure gradually increases to 40 kPa, the bending radius reduces to 60 mm, and it reduces further to 26 mm when the applied

pressure is 80 kPa. The smaller bending radius implies more bending of the trunk. More bending of the trunk would result in a greater forward pull of the leg, allowing the robot to travel further in one bending cycle. The forward motion of the robot in one bending cycle is also determined by the friction between the leg and the wall of the pipe.

The result of the leg friction experiment is shown in Fig. 9. The maximum frictional force recorded for forward motion was 0.14 N, whereas the maximum frictional force during backward motion was -0.27 N. During the forward motion, the spikes on the leg spread out, lowering the contact surface, and thus lowering the frictional force of the leg. On the other hand, during the backward motion, the spikes smooth out and increase the contact area between the leg and the wall. The amount of frictional force depends on the amount of contact area between the leg and the pipe wall in the case of soft rubber contacting a smooth pipe surface. The lower frictional force during the forward pulling of the leg would result in the net forward motion of the robot, as proven in the subsequent experiment.

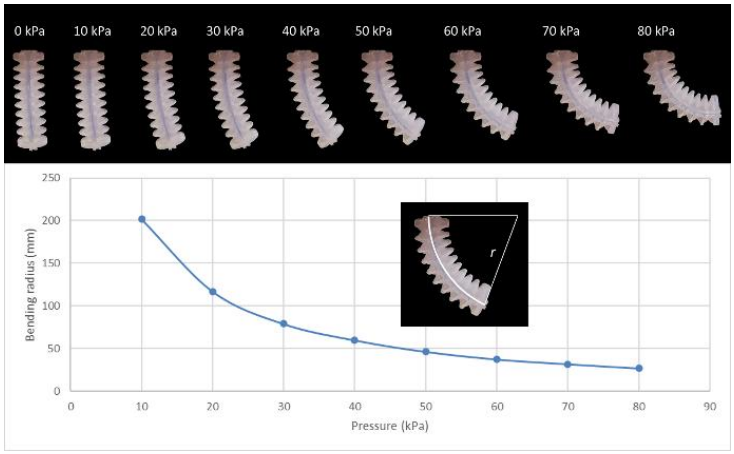

Fig. 8. Trunk's bending radius vs air pressure.

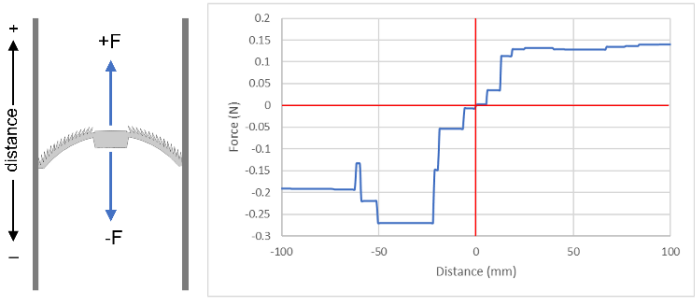

Fig. 9. Leg friction in forward and reverse directions.

Figure 10(a) shows a time-lapse of the lizard soft robot moving through a 50 mm pipe extracted using MATLAB. Figure 10(b), on the other hand, shows the relationship between the speed of the robot and the distance travelled inside the 50 mm diameter pipe. The speed of the robot was calculated using Eq. (2).

At the initial distance of 0 mm, the speed increases and reaches 3 mms^{-1} and slowly fluctuates in speed. The fluctuation in speed was due to the side-to-side bending of the trunk and necks. As stated before, the soft robot moves using the lateral bending of the trunk. When the trunk and necks of the robot bend, the head is pulled slightly backward. This gives the negative speed. The head was pushed forward again when the body and necks straightened, which gave the positive speed value. Throughout the locomotion, the positive speed is greater than the negative speed, which gives the net overall positive speed. The average speed recorded was 2.02 mms^{-1}.

The same experiment was repeated for pipe diameters of 60 mm and 70 mm, and the robot speeds were recorded in Table 1. Figures 11(a) and (b) show a time-lapse of the robot moving inside a 45° and 90° corner, respectively. Both the pipes used are 60 mm in diameter. The navigation speed was measured and calculated from the moment the tip of the robot's head enters the white elbow and emerges from the other end of the elbow. As expected, the robot takes a longer time to move through the 90° corner compared to the 45° corner. This indicates that the sharper angle in the corner gives greater resistance to the forward motion of the robot. Nonetheless, the robot managed to navigate through both corners without a problem.

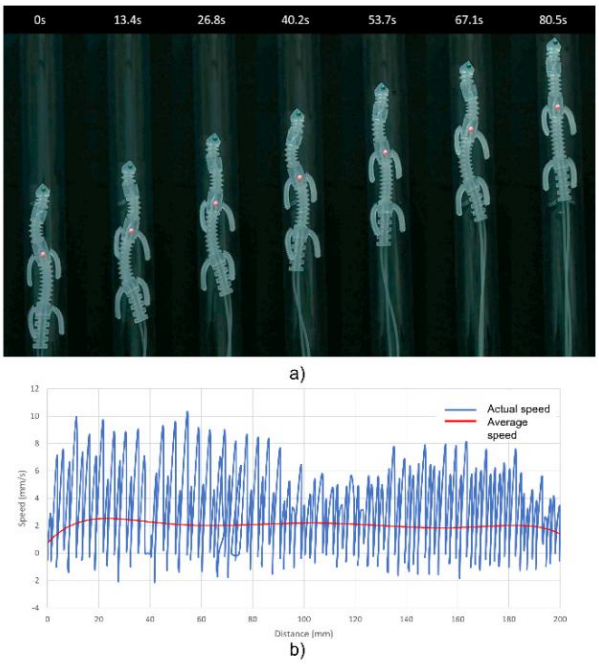

Fig. 10. (a) Time lapse of robot moving through a horizontal straight pipe of 50 mm diameter and (b) speed vs distance of the robot travelling inside a 50 mm diameter pipe (Average speed: 2.02 mms^{-1}).

Table 1 shows the data summary of robot navigation speed inside straight pipes of various diameters and corners of 45° and 90° angles. From the result, it can be observed that the robot moves the slowest inside the 50 mm pipe. This is because, in the 50 mm pipe, the robot has a limited bending radius due to limited operating space. As discussed earlier, the more the trunk bends, the further it can travel in one

step, which means, the higher the robot's speed. However, when moving through a 70 mm pipe, the robot moves slower compared to the 60 mm pipe, despite having more space to bend the trunk. In the 70 mm pipe, while the robot gains more bending radius, it has less friction with the wall and cannot push the body structure of the robot forward.

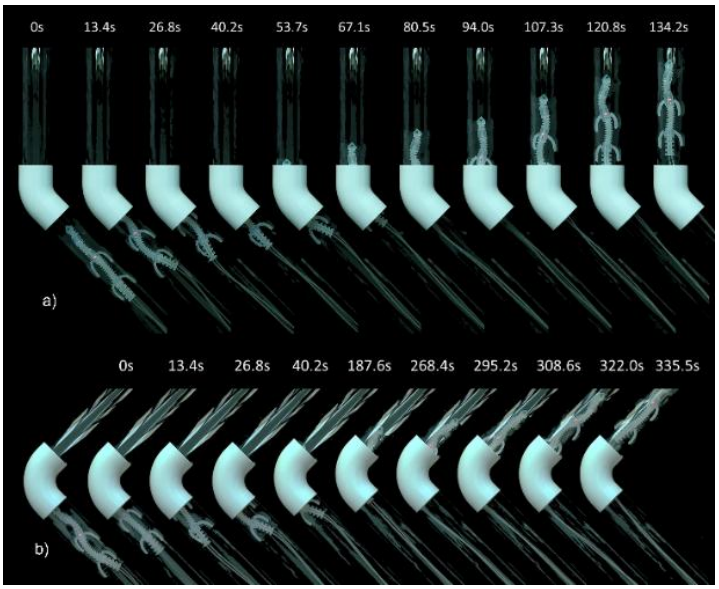

Fig. 11. Time lapsed of the robot moving: (a) inside a 45° and (b) inside a 90° corner pipe of 60 mm diameter.

Table 1. Robot navigation speed inside straight pipe and corners.

Pipe	Straight (Diameter, mm)			Corner	
	50	**60**	**70**	**45°**	**90°**
Speed (mms^{-1})	2.02	2.77	2.33	2.94	0.73

This indicates the importance of friction between the leg of the robot and the wall of the pipe. The robot moves slower when navigating through a 90° corner compared to 45°. This is because the tip of the head takes a longer time to bend to follow the contour of the pipe elbow. Despite the slow movement, the robot does not have any issues moving through a cornered 45° and 90° pipe.

Two parameters have been measured to investigate the head stability of the robot, which are the lateral (side-to-side) movement of the head and shoulder, and the rotation (tilting) of the head and shoulder. The shoulder lateral movement and rotation were measured for comparison purposes to prove the effectiveness of the neck design to improve the stability of the head. Figure 12(a) shows the lateral movement of the head and shoulder of the robot while travelling inside a 50 mm diameter pipe, which was calculated using Eq. (3) from the recorded video. The lateral movement performance of the head and shoulder is almost comparable with the standard deviation of 1.07 mm and 1.49 mm, respectively. However, the slightly

lower standard deviation of the head indicates a slightly higher stability of the head with respect to the lateral movement.

The lateral rotation of the head and shoulder of the robot is shown in Fig. 12(b). From the plot, it can be observed that the head experienced much less lateral rotation as compared to the shoulder, with a standard deviation of 6.6° compared to the standard deviation of 19.8° recorded for the shoulder rotation. The head rotation recorded a maximum rotation of only 12.9° during the robot's navigation, whereas the shoulder part recorded a maximum rotation of 50°. This serves as proof that the neck design has successfully improved the stability of the head of the robot during the in-pipe navigation.

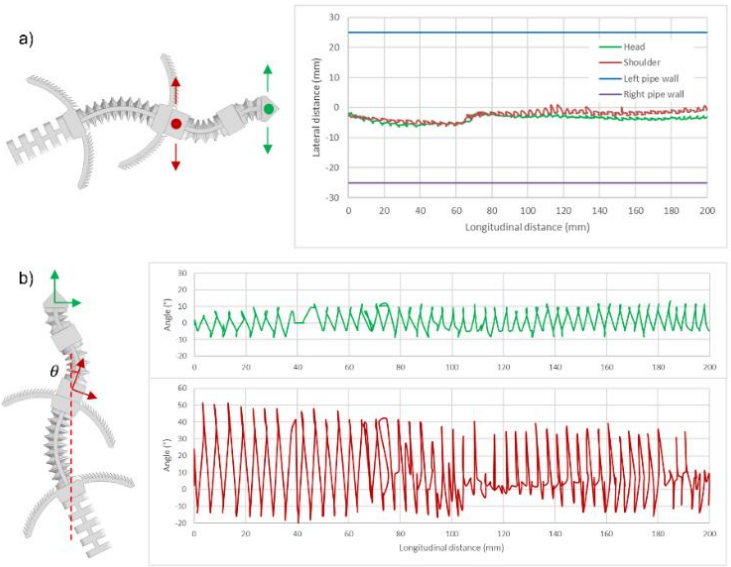

Fig. 12. Results for the head stability test showing (a) the lateral movement and (b) the rotation of the head and shoulder of the soft in-pipe navigation robot.

In general, the current design of the lizard-inspired in-pipe navigation robot has demonstrated its capability to navigate pipes of different diameters and navigate through corners of different angles. However, the speed and the head stability reported in the results are extremely specific to the current size and dimension of the robot and, therefore do not represent the absolute performance value for lizard-inspired in-pipe navigation robot in general. There are many factors that affect robot speed. For this robot, the size of the robot, speed of actuation, leg friction, and diameter of the pipe will affect the speed. If a similar robot is made larger, then it can cover a longer distance in one stroke and is therefore faster as compared to the smaller version. In literature, in-pipe robots come in different sizes and are tested inside pipes of different diameters. In this paper, the comparison was only made on the speed of the robot in several different pipe diameters and corner angles to prove the adaptability of the robot's locomotion.

The current lizard-inspired soft in-pipe robot has several limitations. The current design employs a passive leg to anchor the robot to the wall during

locomotion. The stiffness and length of the legs and the design of the spike on the surface of the leg determine the friction between the wall and the robot, which subsequently determines the strength and the speed of the locomotion. So, currently, there is no active control of this parameter to adapt effectively to different pipe diameters and surface conditions. For the current dimension of the robot, the speed of the locomotion is the highest in the 60 mm diameter pipe and becomes lower as the diameter gets larger or smaller. The current robot design also has no active steering or directional control. During navigation through pipe corners, the robot's head slides against the corner pipe wall, which forces the head and subsequently the body of the robot to bend and follow the direction of the corner. From the results, the larger the corner angle, the slower the robot becomes during cornering. If the wall of the pipe corner is very rough, the robot may get stuck. In addition to that, if the corner radius is small, which does not allow for the robot to turn more gradually, the robot might also get stuck.

4. Conclusion

This paper proposes a lizard-inspired soft in-pipe navigation robot that adopts a lizard's standing wave quadrupedal locomotion strategy with passive legs for navigating inside a pipeline. The whole structure of the robot was constructed from soft and lightweight silicone rubber, allowing the robot to be fabricated at a low cost and can even be made disposable. A series of experiments were conducted to test the performance of the robot, and the results prove that the robot has successfully navigated inside pipes of different diameters and corners of different angles. The current dimension of the robot produces the fastest speed of 2.77 mms^{-1} in 60 mm diameter pipe and slower speeds in pipes with smaller and larger diameters. This suggests that the dimension of the robot influences the range of pipe diameters in which the robot can optimally operate.

The test results on the navigation through corners reveal the influence of corner angle on the speed of the robot. The 90° corner produces a significantly lower speed as compared to the 45° corner, suggesting that the higher the angle of the corner, the more difficult it is for the robot to lizard-inspired robot to navigate. The test on the neck performance also indicates that the neck design managed to stabilize the head of the robot during locomotion with a standard deviation of the head's lateral movement and rotation of 1.07 mm and 6.6°, respectively. The experimental results prove that the lizard-inspired locomotion strategy is a good alternative to other biologically inspired locomotion strategies commonly used in designing an in-pipe navigation and inspection robot.

However, the current design of the lizard-inspired soft in-pipe navigation robot is not without limitations. Hence several improvements can be made to the design of the robot. In future, active legs can be used on the robot instead of the current passive legs, which can potentially improve the friction between the robot and the pipe wall of different diameters. Furthermore, different combinations of soft materials with different shore hardness and different spike designs can be investigated to improve friction. Active steering capability can also be incorporated into the robot to help navigate through a wider range of corner angles effectively.

Acknowledgment

This research is supported by Universiti Sains Malaysia (USM) short-term grant 304/PELECT/6315477.

Nomenclatures

D_{pipe}	Diameter of pipe in mm
$d_{lateral}$	Lateral distance from the centre of pipe
FR_rate	Video frame rate
FR_V_n	Vertical pixel coordinates of the marker in the current frame
FR_V_{n-1}	Vertical pixel coordinates of the marker in the previous frame
H_Co_{marker}	Horizontal pixel coordinates of the marker
$H\_Co_{pipe\_center}$	Horizontal pixel coordinates of the centre of the pipe
l	Trunk length in mm
L_{pipe}	Pipe length in mm
$N\_V_{pipe\_diameter}$	Number of pixels in one diameter of the pipe
$N\_V_{pipe\_length}$	Number of vertical pixels for the entire pipe length
r	Radius of curvature in mm
$v_{vertical}$	Vertical speed in mms^{-1}

Greek Symbols

θ	Angle of curve in degree

Abbreviations

FEA	Finite Element Analysis
PLA	Polylactic Acid

References

1. Roh, S.-g.; Kim, D.W.; Lee, J.-S.; Moon, H.; and Choi, H.R. (2009). In-pipe robot based on selective drive mechanism. *International Journal of Control, Automation and Systems*, 7(1), 105-112.
2. Zhao, W.; Zhang, L.; and Kim, J. (2020). Design and analysis of independently adjustable large in-pipe robot for long-distance pipeline. *Applied Sciences*, 10(10), 3637.
3. Mirats Tur, J.M.; and Garthwaite, W. (2010). Robotic devices for water main in-pipe inspection: A survey. *Journal of Field Robotics*, 27(4), 491-508.
4. Wang, Z.; Cao, Q.; Luan, N.; and Zhang, L. (2010). Development of an autonomous in-pipe robot for offshore pipeline maintenance. *Industrial Robot*: *An International Journal*, 37(2), 177-184.
5. Ab Rashid, M.Z.; Mohd Yakub, M.F.; Zaki Bin Shaikh Salim, S.A.; Mamat, N.; Syed Mohd Putra, S.M.; and Roslan, S.A. (2020). Modeling of the in-pipe inspection robot: A comprehensive review. *Ocean Engineering*, 203, 107206.
6. Verma, A.; Kaiwart, A.; Dubey, N.D.; Naseer, F.; and Pradhan, S. (2022). A review on various types of in-pipe inspection robot. *Materials Today*: *Proceedings*, 50, 1425-1434.
7. Laschi, C.; Mazzolai, B.; and Cianchetti, M. (2016). Soft robotics: Technologies and systems pushing the boundaries of robot abilities. *Science Robotics*, 1(1), eaah3690.
8. Majidi, C. (2019). Soft-matter engineering for soft robotics. *Advanced Materials Technologies*, 4(2), 1800477.

9. Adams, W.; Sridar, S.; Thalman, C.M.; Copenhaver, B.; Elsaad, H.; and Polygerinos, P. (2018). Water pipe robot utilizing soft inflatable actuators. *Proceedings of the* 2018 *IEEE International Conference on Soft Robotics* (*RoboSoft*), Livorno, Italy, 321-326.
10. Zhang, X.; Pan, T.; Heung, H.L.; Chiu, P.W.Y.; and Li, Z. (2018). A biomimetic soft robot for inspecting pipeline with significant diameter variation. *Proceedings of the* 2018 *IEEE/RSJ International Conference on Intelligent Robots and Systems* (*IROS*), Madrid, Spain, 7486-7491.
11. Yamamoto, T.; Sakama, S.; and Kamimura, A. (2020). Pneumatic duplex-chambered inchworm mechanism for narrow pipes driven by only two air supply lines. *IEEE Robotics and Automation Letters*, 5(4), 5034-5042.
12. Mark, A.G.; Palagi, S.; Qiu, T.; and Fischer, P. (2016). Auxetic metamaterial simplifies soft robot design. *Proceedings of the* 2016 *IEEE International Conference on Robotics and Automation* (*ICRA*), Stockholm, Sweden, 4951-4956.
13. Zhang, Z.; Wang, X.; Wang, S.; Meng, D.; and Liang, B. (2019). Design and modeling of a parallel-pipe-crawling pneumatic soft robot. *IEEE Access*, 7, 134301-134317.
14. Verma, M.S.; Ainla, A.; Yang, D.; Harburg, D.; and Whitesides, G.M. (2018). A soft tube-climbing robot. *Soft Robotics*, 5(2), 133-137.
15. Joyee, E.B.; Szmelter, A.; Eddington, D.; and Pan, Y. (2022). 3D printed biomimetic soft robot with multimodal locomotion and multifunctionality. *Soft Robotics*, 9(1), 1-13.
16. Jiang, C.; and Pei, Z. (2021). An in-pipe worm robot with pneumatic actuators based on origami paper-fabric composites. *Textile Research Journal*, 91(23-24), 2724-2737.
17. Calderón, A.A.; Ugalde, J.C.; Zagal, J.C.; and Pérez-Arancibia, N.O. (2016). Design, fabrication and control of a multi-material-multi-actuator soft robot inspired by burrowing worms. *Proceedings of the* 2016 *IEEE International Conference on Robotics and Biomimetics* (*ROBIO*), Qingdao, China, 31-38.
18. Calderón, A.A.; Ugalde, J.C.; Chang, L.; Cristóbal Zagal, J.; and Pérez-Arancibia, N.O. (2019). An earthworm-inspired soft robot with perceptive artificial skin. *Bioinspiration & Biomimetics*, 14(5), 056012.
19. Yeh, C.-Y.; Chen, C.-Y.; and Juang, J.-Y. (2020). Soft hopping and crawling robot for in-pipe traveling. *Extreme Mechanics Letters*, 39, 100854.
20. Ge, J.Z.; Calderón, A.A.; Chang, L.; and Pérez-Arancibia, N.O. (2019). An earthworm-inspired friction-controlled soft robot capable of bidirectional locomotion. *Bioinspiration & Biomimetics*, 14(3), 036004.
21. Gilbertson, M.D.; McDonald, G.; Korinek, G.; Van de Ven, J.D.; and Kowalewski, T.M. (2017). Serially actuated locomotion for soft robots in tube-like environments. *IEEE Robotics and Automation Letters*, 2(2), 1140-1147.
22. Liu, M.; Xu, Z.; Ong, J.J.; Zhu, J.; and Lu, W.F. (2020). An earthworm-like soft robot with integration of single pneumatic actuator and cellular structures for peristaltic motion. *Proceedings of the* 2020 *IEEE/RSJ International Conference on Intelligent Robots and Systems* (*IROS*), Las Vegas, NV, USA, 7840-7845.

23. Quillin, K.J. (1999). Kinematic scaling of locomotion by hydrostatic animals: Ontogeny of peristaltic crawling by the earthworm Lumbricus terrestris. *Journal of Experimental Biology*, 202(6), 661-674.
24. Yamamoto, T.; Konyo, M.; and Tadokoro, S. (2015). A high-speed locomotion mechanism using pneumatic hollow-shaft actuators for in-pipe robots. *Proceedings of the* 2015 *IEEE/RSJ International Conference on Intelligent Robots and Systems* (*IROS*), Hamburg, Germany, 4724-4730.
25. Seok, S.; Onal, C.D.; Cho, K.-J.; Wood, R.J.; Rus, D.; and Kim, S. (2013). Meshworm: A peristaltic soft robot with antagonistic nickel titanium coil actuators. *IEEE/ASME Transactions on Mechatronics*, 18(5), 1485-1497.
26. Kamata, M.; Yamazaki, S.; Tanise, Y.; Yamada, Y.; and Nakamura, T. (2018). Morphological change in peristaltic crawling motion of a narrow pipe inspection robot inspired by earthworm's locomotion. *Advanced Robotics*, 32(7), 386-397.
27. Tang, Z.; Lu, J.; Wang, Z.; Ma, G.; Chen, W.; and Feng, H. (2020). Development of a new multi-cavity pneumatic-driven earthworm-like soft robot. *Robotica*, 38(12), 2290-2304.
28. Das, R.; Murali Babu, S.P.; Palagi, S.; and Mazzolai, B. (2020). Soft robotic locomotion by peristaltic waves in granular media. *Proceedings of the* 2010 3rd *IEEE International Conference on Soft Robotics* (*RoboSoft*), New Haven, CT, USA, 223-228.
29. Digumarti, K.M.; Conn, A.T.; and Rossiter, J. (2018). EuMoBot: Replicating euglenoid movement in a soft robot. *Journal of The Royal Society Interface*, 15(148), 20180301.
30. Niu, H.; Feng, R.; Xie, Y.; Jiang, B.; Sheng, Y.; Yu, Y.; Baoyin, H.; and Zeng, X. (2021). Magworm: A biomimetic magnet embedded worm-like soft robot. *Soft Robotics*, 8(5), 507-518.
31. Takayama, T.; Takeshima, H.; Hori, T.; and Omata, T. (2015). A twisted bundled tube locomotive device proposed for in-pipe mobile robot. *IEEE/ASME Transactions on Mechatronics*, 20(6), 2915-2923.
32. Hu, F.; and Li, T. (2021). An origami flexiball-inspired metamaterial actuator and its in-pipe robot prototype. *Actuators*, 10(4), 67.
33. Schiller, L.; Seibel, A.; and Schlattmann, J. (2019). Toward a gecko-inspired, climbing soft robot. *Frontiers in Neurorobotics*, 13, 106.
34. Tang, Y.; Zhang, Q.; Lin, G.; and Yin, J. (2018). Switchable adhesion actuator for amphibious climbing soft robot. *Soft Robotics*, 5(5), 592-600.
35. Farley, C.T.; and Ko, T.C. (1997). Mechanics of locomotion in lizards. *Journal of Experimental Biology*, 200(16), 2177-2188.
36. Aerts, P.; Van Damme, R.; Vanhooydonck, B.; Zaaf, A.; and Herrel, A. (2000). Lizard locomotion: How morphology meets ecology. *Netherlands Journal of Zoology*, 50(2), 261-277.